An experimental setup for creating and imaging $^4\mathrm{He}_2^*$ excimer cluster tracers in superfluid helium-4 via neutron-^{3}He absorption reaction ᴱᴾ

V. Sonnenschein [iD], Y. Tsuji, S. Kokuryu, W. Kubo, S. Suzuki, H. Tomita [iD], Y. Kiyanagi, T. Iguchi, T. Matsushita [iD], N. Wada, M. Kitaguchi, H. M. Shimizu, K. Hirota, T. Shinohara [iD], K. Hiroi, H. Hayashida, W. Guo, D. Ito, and Y. Saito

COLLECTIONS

View Online **Export Citation** **CrossMark**

ARTICLES YOU MAY BE INTERESTED IN

An experimental setup for creating and imaging ⁴He₂* excimer cluster tracers in superfluid helium-4 via neutron-³He absorption reaction

View Online   Export Citation   CrossMark

V. Sonnenschein,[1,a] ⓘ Y. Tsuji,[1] S. Kokuryu,[1] W. Kubo,[1] S. Suzuki,[1] H. Tomita,[1] ⓘ Y. Kiyanagi,[1] T. Iguchi,[1]
T. Matsushita,[2,b] ⓘ N. Wada,[2] M. Kitaguchi,[2] H. M. Shimizu,[2] K. Hirota,[2] T. Shinohara,[2] ⓘ K. Hiroi,[3]
H. Hayashida,[4] W. Guo,[5,c] D. Ito,[6] and Y. Saito[6]

AFFILIATIONS

[1] Department of Energy Engineering, Nagoya University, Nagoya, Aichi 464-8603, Japan
[2] Department of Physics, Nagoya University, Nagoya, Aichi 464-8602, Japan
[3] J-PARC Center, Japan Atomic Energy Agency, Tokai, Ibaraki 319-1195, Japan
[4] Comprehensive Research Organization for Science and Society, Tokai, Ibaraki 319-1106, Japan
[5] National High Magnetic Field Laboratory, Tallahassee, Florida 32310, USA
[6] Institute for Integrated Radiation and Nuclear Science, Kyoto University, Kumatori, Osaka 590-0494, Japan

[a] Author to whom correspondence should be addressed: volker@nagoya-u.jp
[b] matsushita@cc.nagoya-u.ac.jp
[c] Also at: Mechanical Engineering Department, Florida State University, Tallahassee, Florida 32310, USA.

ABSTRACT

For the purpose of future visualization of the flow field in superfluid helium-4, clusters of the triplet state excimer $^4\text{He}_2{}^*$ are generated along the micro-scale recoil tracks of the neutron-absorption reaction $n + {}^3\text{He} \rightarrow {}^3\text{T} + p$. This reaction is induced by neutron irradiation of the ^3He fraction contained in natural isotopic abundance liquid helium with neutron beams either from the Japan Proton Accelerator Research Complex, Materials and Life Science Experimental Facility (JPARC)/Materials and Life Science Experimental Facility or from the Kyoto University Institute for Integrated Radiation and Nuclear Science. These $^4\text{He}_2{}^*$ clusters are expected to be ideal tracers of the normal-fluid component in superfluid helium with several advantageous properties. Evidence of the excimer generation is inferred by detection of laser induced fluorescence emitted from the $^4\text{He}_2{}^*$ clusters excited by a purpose-built short pulse gain-switched titanium:sapphire (Ti:sa) laser operating at a wavelength of 905 nm. The setup and performance characteristics of the laser system including the Ti:sa and two continuous wave re-pumping lasers are described. Detection at the fluorescence wavelength of 640 nm is performed by using optical bandpass filtered photomultiplier tubes (PMT). Electrical noise in the PMT acquisition traces could successfully be suppressed by post-processing with a simple algorithm. Despite other laser-related backgrounds, the excimer was clearly identified by its fluorescence decay characteristics. Production of the excimer was found to be proportional to the neutron flux, adjusted via insertion of different collimators into the neutron beam. These observations suggest that the apparatus we constructed does function in the expected manner and, therefore, has the potential for groundbreaking turbulence research with superfluid helium.

Published under license by AIP Publishing. https://doi.org/10.1063/1.5130919

I. INTRODUCTION

Turbulence is an important phenomenon in non-equilibrium systems that is still not fully understood, even for canonical flows.[1–4] In order to enrich our understanding of turbulence, in general, there is now a growing interest in the field of Quantum Turbulence[5–8] (QT), which is commonly present in superfluids such as superfluid helium and Bose Einstein condensates (BECs).[9] Superfluid or QT behavior may also be present in exotic matters, such as the core of neutron stars[10,11] or in high energy particle collisions[12]

and galactic cold dark matter halos that are believed to form BECs.[13] So far, ^{4}He has been utilized in the majority of the QT research due to its availability and ease of preparation.

Below the lambda-point T_λ at 2.172 K, ^{4}He transitions from its classical liquid phase into a superfluid phase (He II). In the temperature range from 1 K to T_λ, the flow in He II can be phenomenologically described by a two-fluid model,[14,15] consisting of normal and superfluid components, which can flow independently from one another. The superfluid component is attributed to the condensation of the bosonic ^{4}He atoms to the lowest energy ground state as in the formation of a BEC. One defining characteristic of superfluids is the existence of stable topological defects, i.e., the quantized vortex lines, each of which carries a single quantum of circulation. These vortices can scatter on the thermal excitations making up the normal component, resulting in a "mutual friction" between the two components. The dynamics and interaction among the quantized vortices (vortex tangles) as well as the effect of mutual friction are the key topics of QT.[6]

So far, micro-particle tracers made from frozen hydrogen[16] or polymer[17] have been used for flow visualization using particle image velocimetry (PIV)[18] or particle tracking velocimetry.[19] However, due to their micrometer size, which is substantially larger than that of the vortex core, these tracers can interact strongly with both the viscous normal fluid and the quantized vortices in the superfluid, which makes their motion hard to interpret, especially for flows where the two fluids have different velocity fields. The long lived (13s) triplet state of the ^{4}He$_2$* excimer is a new class of tracers that may alleviate this issue.[20] These excimer molecules can be generated by various means such as electrical discharges or the use of intense laser fields.[21] By creating a cloud of ions and excited atoms, the ^{4}He$_2$* molecules are formed via collisions and recombinations. Their beneficial properties include[22] a small size of few angstroms, neutrality, being non-aggregating, as well as the possibility of imaging via laser-induced fluorescence (LIF). Furthermore, they follow only the normal flow above 1 K[23] and can be trapped on vortex lines below 0.6 K.[24]

Two-photon excitation at 905 nm from the triplet ^{4}He$_2$* ground state ($a^3\Sigma_u^+$) to the $d^3\Sigma_u^+$ state yields fluorescence at 640 nm by decay to the $b^3\Pi_g$ state.[25,26] After fluorescence, the molecule may get trapped in vibrational states with a lifetime of >100 ms so that repumping lasers at 1073 nm and 1099 nm have to be employed for a quick return to the ground state and repetition of the cycle. Due to the two-photon nature of the excitation transition, a short, few ns pulse duration laser with an energy density of about 1 mJ/cm^2 is needed for saturating the fluorescence. The two-photon transition is near-resonant to the intermediate $c^3\Sigma_g^+$ state at 910 nm, whose lifetime is also expected to be shorter than 20 ns.[27] An alternative method may be the use of a transition at 465 nm,[28,29] which could be interrogated using a continuous-wave laser. In this case, however, the pump and fluorescent light are at the same wavelength, requiring a setup minimizing the scattering of the pump radiation.

Until now, the cycling transition laser-driven fluorescence scheme for detecting ^{4}He$_2$* excimers has not been pushed to the limit for imaging individual excimers. Instead of individual tracking, it is desired to develop a method to produce many small clouds of ^{4}He$_2$* excimers in He II and then treat each cloud as one "tracer." Such tracer clouds would allow for full-space velocity field

measurement using conventional PIV and PTV methods. In this study, we utilized the neutron absorption reaction on natural occurring ^{3}He within He II: n + ^{3}He → ^{1}H + ^{3}H + 764 keV, which creates a cluster of ^{4}He$_2$* along the micro-scale recoil tracks of the ^{1}H and ^{3}H particles. The tracks have a length of about 100 μm, resulting in a cluster size, which may, in many cases, be larger than the so-called quantum length scale l_q,[30] defined as the average distance between quantized vortices. However, the fact that these clusters are made of the much smaller individual excimer particles, should still allow us to infer interesting quantum effects by observing the deformation and broadening of the clouds. Each recoil event is estimated to result in the production of about 10^4 ^{4}He$_2$* excimers in the metastable triplet state[31] via a recombination process of ions, electrons, and metastable helium atoms.[32] Our experiments were carried out at the Kyoto University Reactor (KUR) and the Materials and Life Science Experimental Facility (MLF) beam-line 22 (BL22) of the Japan Proton Accelerator Research Complex (J-PARC). A summary of the preliminary results was reported in our previous conference paper,[31] displaying solid evidence for ^{4}He$_2$* generation by neutrons. The purpose of this manuscript is to give a more detailed description of the experiments with a focus on the laser setup and a more in-depth data-analysis. This paper is organized in the following way. In Sec. II, the laser system, including the gain-switched Ti:sapphire excitation laser and the re-pumping lasers, the helium Dewar, and the detection setup are covered. Additionally, the important characteristics of the neutron facilities at the KUR and J-PARC are described. Experimental procedures, data processing, filtering, and analysis are given in Sec. III. In Sec. IV, the results of the analysis are discussed, concluding with a summary and outlook (Sec. V) on an upcoming experiment aimed at imaging the excimer clusters.

II. EXPERIMENTAL DETAILS

A general layout of the experimental setup is displayed in Fig. 1. The laser system including pump laser head was arranged on a 60 × 70 cm^2 optical breadboard, allowing for easy transportability and quick setup at the experimental facilities, only requiring some fine realignment for power maximization. Using the cross of a laser alignment tool, the neutron beam collimation slits and the laser path direction were first aligned, after which the Dewar was carefully placed in-between with a heavy duty motorized 3-axis positioning platform. Only limited time (typically 1 day) was available for the preparation of all components such as laser system, optical Dewar, and detection systems before the start of an experimental run.

A. Ti:sapphire laser

The operation of the laser system is an important part to fully understand the data-acquisition process as well as the following data processing, systematic issues, and error estimates. Additionally, the titanium:sapphire (Ti:sapphire) laser system described here—while not based on any new technology—uses a quite simple design, which may be of interest for other applications or laboratories. Commercial systems for 905 nm based on Ti:sapphire or optical parametric oscillation (OPO) are available; however, most would not have the compact dimensions required, so it was decided to reuse an existing
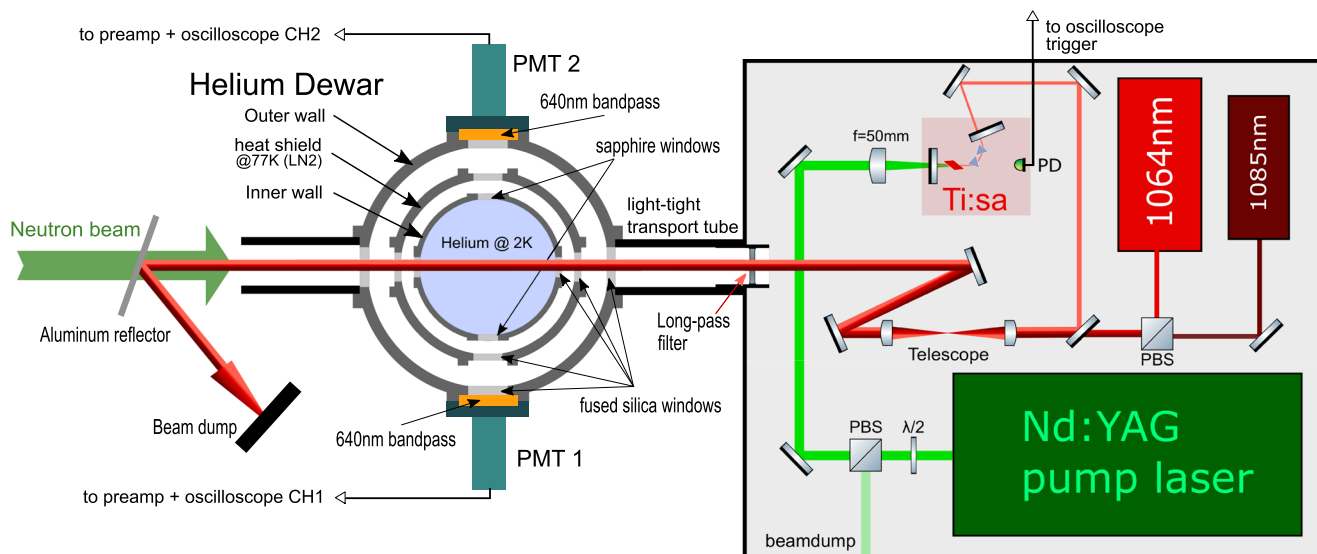
FIG. 1. Layout of the experimental setup at the J-PARC, including the laser system consisting of Nd:YAG pump laser, Ti:sapphire laser, and two continuous wave repumping lasers, as well as the optical helium Dewar and PMTs for fluorescence acquisition.

532 nm Nd:YAG pump laser, simply using a self-built Ti:sapphire cavity as a compact wavelength converter.

An overview of the complete laser setup, including the Nd:YAG pump, Ti:sa laser, and the two continuous wave (cw) lasers for repumping, is shown in Fig. 1. To generate the required high intensity laser pulse at 905 nm, a Ti:sapphire laser was designed and characterized. While Ti:sapphire lasers with short pulse duration can be achieved using active Q-switching by Pockels cells or with mode-locking techniques, these designs often come with considerable complexity and/or space requirements. We chose the alternative route of a simple two-mirror gain-switched cavity design with a simple rendering of the computer aided design (CAD) design, as shown in Fig. 2. Similar designs have been reported,[33–35]
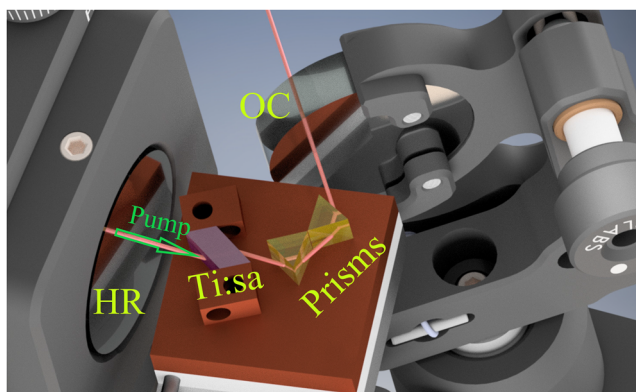

FIG. 2. Rendering of the Ti:sapphire laser geometry. Prisms and laser crystal are oriented at the Brewster angle. The pump beam is incident from the left.

even demonstrating sub-ns performance, however, not involving wavelength-tunable operation far from the gain-maximum of Ti:sapphire as required here. A short few ns duration output pulse was achieved by combination of small cavity dimensions (optical path length: 4 cm) and a short pump pulse. A low repetition-rate (15 Hz) flash-lamp pumped Nd:YAG (New Wave Research, Solo PIV 15) with a measured maximum pulse energy of 10.5 mJ and a pulse duration of 5 ns was used as a pump source. A combination of $\lambda/2$-waveplate and polarization beam splitter (PBS) cube allowed varying the pump energy, after which it was focused by a f = 50 mm plano–convex lens into the Ti:sapphire cavity. The cavity high reflector (HR) had high transmission at the pump wavelength and a reflectivity R > 99.8% from 850 nm to 1050 nm, while the output coupler (OC) covered the same range with ≈20% transmission. Tuning of the center wavelength was realized by the inclusion of two 5 mm N-SF11 prisms (P1 and P2). The wavelength was selected by fine rotation of the OC. A drawback of this was a slight angular steering of the output beam with the wavelength. Both the Ti:sapphire crystal (CR, GTAT Corporation, 4 mm, FOM = 150, $\alpha_{532} = 5.5$ cm^{-1}) and prisms were oriented at close to Brewster angle of incidence in order to keep Fresnel losses of the polarized beams to a minimum. The crystal was held in a small mounting structure on top of a copper plate onto which the two prisms were glued with epoxy for long-term stability after initial rough alignment using a 850 nm laser pointer module (Thorlabs, CPS850S). As the application did not demand a high beam quality output, a simple plane–plane geometry in conjunction with gain guiding[36] effects was found to be sufficient.

In order to stay below the optical damage threshold, the pump focus was located behind the crystal, about half-way to the first prism, as indicated in Fig. 3. Due to the Brewster angle, the pump spot size on the crystal surface can be assumed to be elliptical with estimated dimensions of 0.3 × 0.5 mm^2, equating to a fluence of
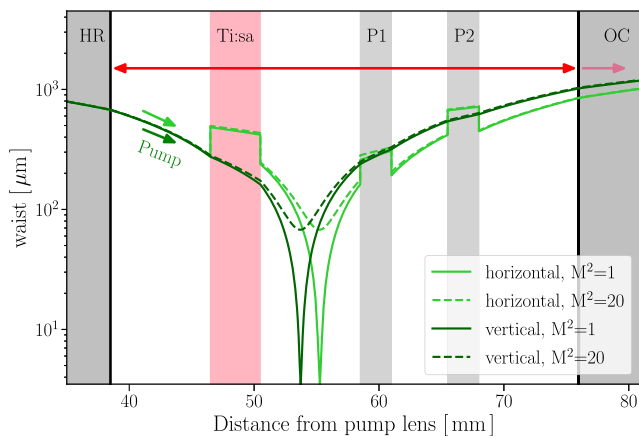
FIG. 3. Pump-mode propagation through the Ti:sa laser cavity. The pump intensity on optical surfaces is nearly independent of beam-quality (M^2 value).

FIG. 4. Performance characteristics of the Ti:sapphire laser system depending on pump pulse energy, showing the output energy, FWHM pulse duration, and time delay with respect to pump pulse for four different wavelengths.

about 1 J/cm^2 at a pulse energy of 5 mJ. The pump beam propagation was calculated for two different M^2 beam quality factors, showing that the fluence on the optical surfaces only varied by a negligible amount. This, in effect, makes the operation insensitive to pump beam quality, which was not well known beforehand. Nevertheless, the short pump pulse duration restricts the safe operating range.

The performance characteristics of the laser at several wavelength settings are shown in Fig. 4. A FWHM pulse duration around 3.5(10) ns and an output energy close to 0.8 mJ at 905 nm were achieved at an input energy of 5.8 mJ. As this was deemed sufficient for the first experiments, the maximum available pump power of 11 mJ was not applied in order to minimize the risk of optical damage before the start of the experiment. Thus, it is likely that better performance can still be achieved if desired. The pulse duration of the Ti:sapphire laser was acquired with a fast biased silicon photodiode detector with a specified rise/fall time of 1 ns. The measured pulse is the convolution of the detector response and the laser pulse shape, which was already taken into account in the results. However, lacking an experimentally measured impulse response of the detector, an error of 1 ns was assumed. The delay between pump- and output pulse peak varied from 150(20) ns near the threshold to about 28.0(5) ns at the maximum energy at 905 nm with the errors given by the timing jitter.

B. Repumping lasers and beam transport

The two cw lasers at 1064 nm (BeamQ, <1000 mW, DPSS) and 1085 nm (CNI MIL-III-1085, 50 mW, diode laser) were used for repumping purposes. Although their wavelengths did not match exactly to the literature values,[25] the strong collisional broadening of transitions in liquid He substantially relaxes the wavelength precision requirements. An exemplary spectrum of the two repumping lasers and the Ti:sa laser, measured with a USB spectrometer (Lasertack, LR2), is shown in Fig. 5. The repump lasers had opposite polarization at their respective outputs so that they could be spatially overlapped using a polarizing beam splitter (PBS) cube without the inclusion of a $\lambda/2$-waveplate. They were then further combined with the Ti:sapphire laser using a dichroic mirror (Thorlabs, DMLP950)
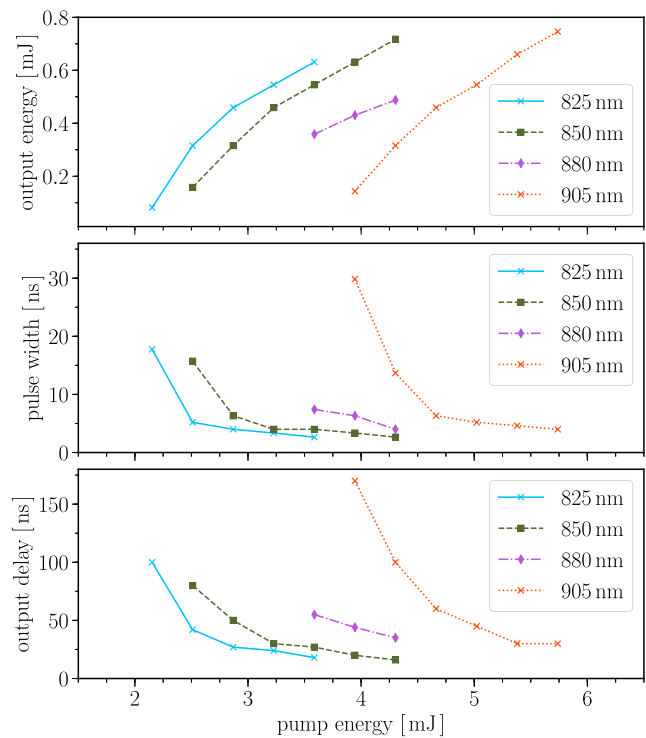
and subsequently collimated with a telescope. Moving the second lens of the telescope allowed for adjusting the spot size at the Dewar center. The beam profile shape and collimation of the 1064 nm laser were noticeably worse, resulting in about two times larger beam-spot compared to the other lasers.

FIG. 5. Optical spectrum of the three laser sources. Given are the peak-positions λ_{1-3} and Gaussian widths σ_{1-3} of the curve fit (red line).

After the telescope, the beams passed a long-pass filter with a cutoff wavelength of 735 nm (Thorlabs, DMLP735) and entered into a light-tight transport tube, sealed by thick black tape. The long-pass fi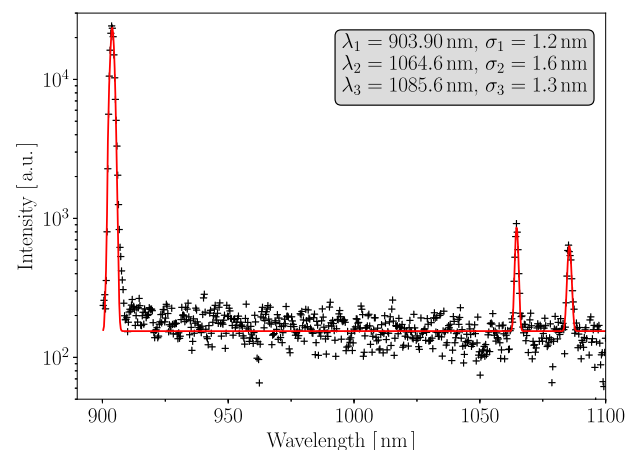lter prevents both the transmission of radiation from the scattered light of the 532 nm pump pulse and spontaneous fluorescence from the Ti:sa crystal, which has significant contributions down to a wavelength of 620 nm. Both of these sources could easily interfere with the detection of the excimer fluorescence. To minimize neutron activation of laser components, only one pick-up mirror and the long-pass filter were in direct line-of-sight of the neutron beam.

A stainless steel Dewar was used for the experiment with an outer diameter of 30 cm and an inner diameter of 16 cm, which was filled with liquid helium. The thermal shield of the Dewar was cooled by LN_2 to 77 K, and the temperature of the liquid helium was lowered by evaporation, cooling using a vacuum pump (Kashiyama NeoDry36E, 600 l/min at the J-PARC and AnnestIwata ISP-250B, 300 l/min at the KUR) to about 1.8–1.9 K in order to reach below the λ-point. An exemplary temperature and pressure trend during the experiments of one day is shown in Fig. 6. Due to the evaporation of helium, only a time-window of about six hours was available before the Dewar had to be refilled. To reach the center of the Dewar, the laser light passed through three windows. The windows were made of uncoated fused silica, resulting in expected transmission losses caused by Fresnel reflection of about 18% to the center and 33% through all six windows. Beyond the Dewar, the laser light was either blocked directly with black tape or aluminum coated tape (KUR expt.) or passed through another transport tube (J-PARC expt.), after which it was first deflected by using a thin aluminum plate and finally reached a beam-dump.

C. Neutron beams

The neutron beam at KUR experiments was a reactor generated continuous beam with a flux of 8.5×10^7 (n/s)/cm² at an operating power of 5 MW.[37] The peak of the energy distribution was at
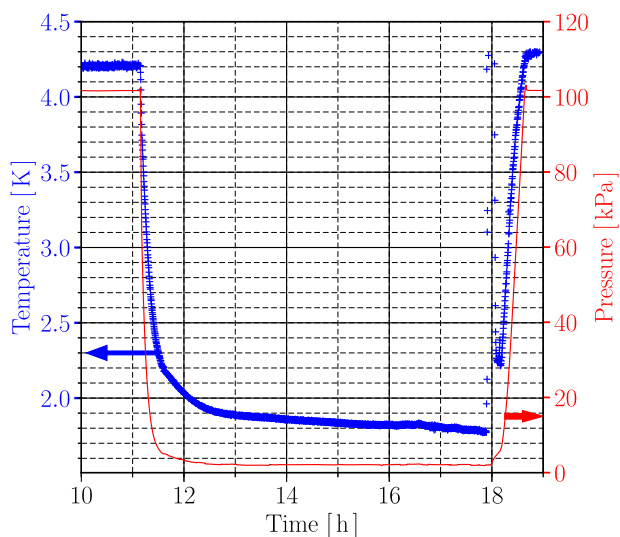

FIG. 6. Temperature and pressure trend during one experimental day.

0.057 eV with a width from 0.013 to 0.23 eV at 1/10th peak height. In contrast, the neutron source at the J-PARC was generated by a pulsed proton beam impinging on a target followed by moderators to generate a cold neutron beam. The source operates at a pulse repetition rate of 25 Hz, thus effectively performing as a continuous source in our experiment considering the lifetime of 13 s of the excimer. Its time-integrated neutron flux was 6.9×10^6 (n/s)/cm² at 400 kW proton beam intensity, with an energy range from 0.0016 eV to 0.36 eV. During the proton pulse, the neutron beam is accompanied by gamma radiation, which may influence the excimer generation rate, an effect which has already been considered in Ref. 31. The neutron flux at the J-PARC could be adjusted via different opening diameter settings of the main shutter and a rotary collimator, as listed in Table I. By combination, the flux intensity could be adjusted in a wide range from 0.5% to 100% of the maximum. A rectangular slit collimator before the Dewar with a size of either 20×20 mm² or 40×40 mm² can be applied to minimize the irradiation of the helium Dewar. For a neutron flux of $0.36 \cdot 10^6$/(s cm²), an excimer generation rate of 22/(s cm³) was calculated.[31] Suppression of the neutron beam can be performed by inserting a blocker made of boron carbide (B_4C) and polyethylene.

D. Electronics and data acquisition

Two additional viewports of the helium Dewar, oriented perpendicular to the laser and neutron beams, were used for fluorescence detection with photomultiplier tubes (PMTs). The inner windows on the detector sides were made of sapphire, slightly increasing transmission losses as compared to the laser-path to about 25%. The two PMTs from Hamamatsu Photonics had differing specifications for the quantum efficiencies at the fluorescence wavelength ε_{640} and signal rise times τ_r. They were equipped with a T > 95% bandpass-filter (No. 65–107, Edmund Optics) at 640 ± 10 nm with an optical density OD > 4 suppression at the laser wavelengths. Both PMT-1 (R750 H6520MOD, $\tau_r = 2.5$ ns, $\varepsilon_{640} = 0.5\%$, and $\varnothing$15 mm) and PMT-2 (H10426-01MOD, $\tau_r = 15$ ns, $\varepsilon_{640} = 25\%$, and $\varnothing$25 mm) outputs were fed into a preamplifier (preamp: KUR only) before being transported with 5–10 m long BNC cables to a high speed digital oscilloscope (Tektronix, DPO7254) in a radiation-safe area. Three channels, consisting of PMT 1, PMT 2, and the laser photodiode, were acquired using the oscilloscope. The rising edge of the PD signal at about half peak-height was used as a trigger signal. At a time-resolution of 100 ps and with 5000 data points per trace, a time-span of 500 ns was covered for each laser shot with 100 ns of pre-trigger capture included. A single acquisition typically contained the traces for 500 or 2000 laser shots, equating to a time-period of about 30 s or 2 min based on the repetition rate of the laser.

TABLE I. Neutron flux ratios estimated for different collimator diameter settings.

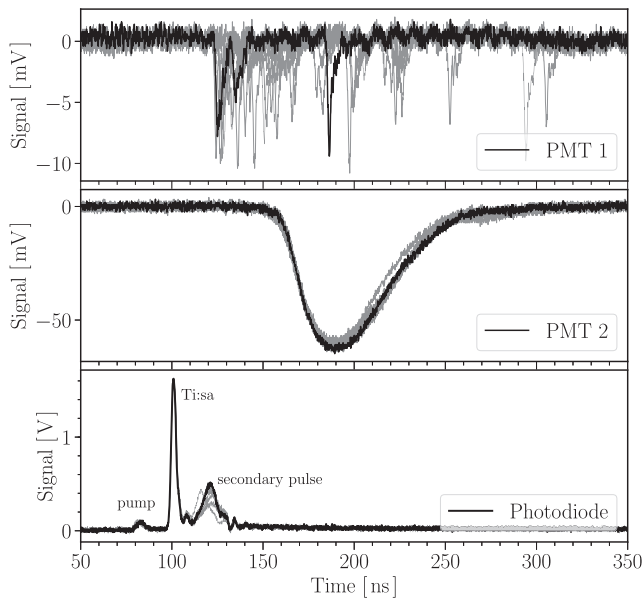|	Diameters (mm)	Flux [10^6/(s cm²)]
Main shutter	100/50.1/26.4	6.9/2.07/0.66
Rotary coll.	100/15	6.9/0.36

FIG. 7. Traces of the oscilloscope signals of PMT 1, PMT 2, and the photodiode. Multiple traces in gray indicate the shot-to-shot variation of the signals.

III. DATA ANALYSIS

Typical oscilloscope traces of all channels are shown in Fig. 7. The black lines show the data of a single trigger event, while the gray lines display the data of 10 events reflecting the shot-to-shot variation. The photodiode signal exhibits three distinct peaks. The first small peak corresponds to the pump laser pulse, the second peak corresponds to the main Ti:sapphire laser pulse, and the third is a secondary parasitic emission pulse of the Ti:sa laser, whose

origins are likely similar to those discussed in Ref. 33, where localized variations in the pump beam intensity cause different pulse build-up durations. This secondary pulse was notably weaker, with longer pulse duration and depended on the alignment of the Ti:sa cavity. It was most apparent at high pump energies and alignment optimized for the maximum output power. As the primary goal of the first measurements was only to verify excimer generation, an attempt to minimize this parasitic pulse was only performed near the end of the measurement run.

A. PMT signal conditioning

The signal of PMT 2 was found to be strongly saturated due to its high efficiency and longer response time, showing insignificant change when changing laser power or the neutron beam was turned on. On the other hand, PMT 1 was not saturated, and a clear effect of the neutron beam on the photon incidence rate was seen. While at low neutron flux, the incidence rate was low enough to possibly attempt photon counting, at high flux, many pile-up events occurred so that the analog signal was used in data analysis.

The raw PMT signal traces contained a small electrical noise component, which stemmed from the HV Q-switch of the Nd:YAG pump laser. Since the PMT data-acquisition was triggered on the Ti:sa laser output, not on the pump laser itself, this noise was exhibiting the same timing jitter as was present between the two lasers. Furthermore, estimation of the noise component from a single shot acquisition proved difficult as it usually included real photon signals as well as noise. However, as the photon events were distributed in time—fluctuating from shot to shot—each trace contained some region without the influence of photon signals. In the data acquired at the KUR, there was an additional issue due to impedance mismatch between preamplifier and oscilloscope, causing reflections of the signals. The noise background was, therefore, estimated by analyzing each whole set of acquisitions in the following manner, as visualized in Fig. 8. First, by adding a time-shifted fraction of the
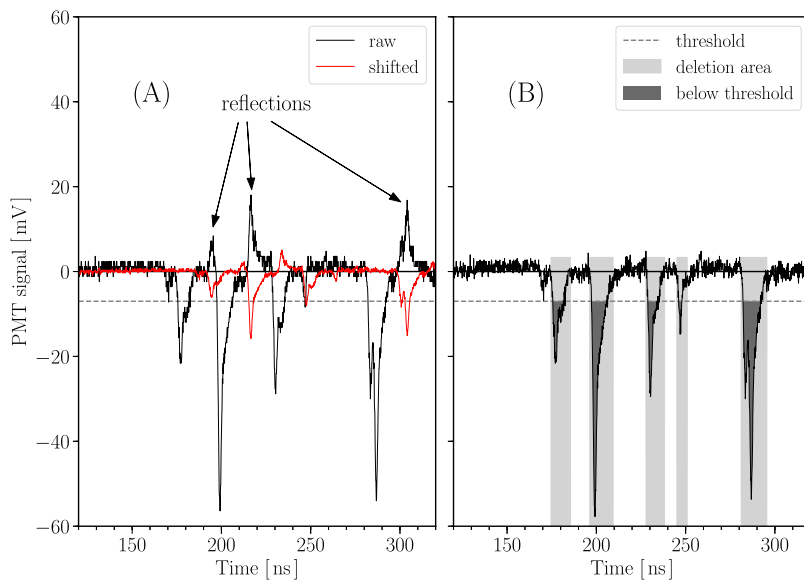

FIG. 8. PMT acquisition trace analysis. (a) Signal reflections caused by impedance mismatch are compensated, as detailed in the text. (b) The dashed line indicates the discrimination threshold level. The light shaded areas mark the regions where data points are ignored to allow the estimation of the noise background.

signal to itself the reflections in the KUR, data were suppressed, as indicated on the left-hand side of Fig. 8(a). The black line is the raw signal, while the red line shows the raw signal shifted by about 17 ns to the right and multiplied by a factor 0.28 to account for the attenuation of the reflected signal. This resulted in the reflection-free signals on the right-hand side of Fig. 8(b). As next step, each individual PMT trace was analyzed to find the positions of photon signals. For this purpose, a simple discriminator condition was set so that a photon incidence was assumed in case the PMT signal dropped below a fixed threshold (dark shaded area). To accommodate for rise and fall time constants of the PMT, a span of 3 ns/9 ns before and after reaching the threshold was additionally selected (light shaded region). Finally, the points in the selected regions were removed (weights set to zero) and the remaining data-points of all traces averaged. A similar technique is used in photo-manipulation, where multiple photographs of a crowded sight-seeing spot are taken so that by post-processing with a median filter, distracting fore-ground objects (such as tourists) can be removed. Before the final averaging, each trace was slightly time shifted in order to compensate variation within the pump-pulse timing. While only a minor adjustment, it further improved the noise estimation, especially for low pump energy, where the timing jitter was larger. In a few cases, when the pump pulse timing was not measurable due to the insufficient photodiode signal, this step was omitted.

The result of this procedure is displayed in Fig. 9. However, the raw signal average (red curve) is noticeably affected by noise, after subtraction of the calculated noise (black curve), the corrected signal (blue curve) has only minor fluctuations. The observed double-peak structure was related to the Ti:sapphire laser double-pulsing output. The calculated noise signal shows a combination of high- and lower-frequency noise, with the higher frequency components decaying
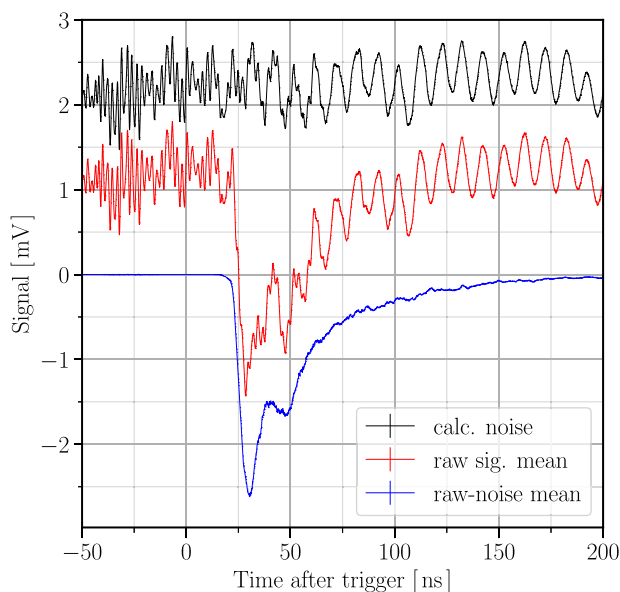

FIG. 9. Comparison of mean raw signal and mean corrected signal. Subtraction of the extracted noise from the raw signal yields a considerable improvement in signal quality. Curves are offset for clarity.

quicker, not being present in the tail of the fluorescence signal. It was further investigated, whether the noise signal changed over the course of the experiment. While slight variation was found in a single set of acquisitions, noticeable changes were observed over longer periods of time or after adjusting experimental settings.

Finally, to remove other non-excimer related background, acquisitions with neutron beam turned off (n_{Off}) were subtracted from those with neutron beam turned on (n_{On}). The total integrated PMT signal was then calculated, as well as the time constant of the fluorescence decay fitted. Several experimental parameters, such as neutron beam flux, excitation laser intensity, spot-size, wavelength, and operation of the repumping lasers, were varied during the experiment.

IV. RESULTS

A. Decay time constant and J-PARC vs KUR comparison

Two representative results from the KUR and the J-PARC experimental runs are shown in Figs. 10 and 11, respectively. They show the sum of the results of a single day of acquisitions equating to the total fluorescence signal of about 6000 (KUR) and 8000 (J-PARC) laser pulses. The quality of the data acquired at the KUR was significantly lower, yielding a contrast ratio n_{On}/n_{Off} of about 5–10 between the signal with neutron beam turned on and with neutron beam turned off, compared to a ratio of up to 50 in the J-PARC data. Several issues may be blamed for this lower performance such as the use of only a single repumping laser (1085 nm) at the KUR instead of two at the J-PARC or the lower pulse energy of the Ti:sapphire laser (0.4–0.6 mJ vs 0.6–0.8 mJ), but these are unlikely to have such a large effect, as shown later. In both experiments, a fluorescence signal was observed even for "n_{Off}" setting during laser-pulse incidence. However, while this background did decay quickly at the J-PARC, at the KUR, a slower decay contribution was observed, with a similar time-constant as the expected $^4He_2{}^*$ signal. A possible reason for this signal could be the use of black tape as beam-block near the exit window of the Dewar, as discussed in Sec. II B. At high laser intensities, many absorbing materials such as the tape or contaminants on its surface may emit broadband fluorescence or black-body light with unknown properties. Additionally, the tape may partially reflect the laser beam back into the Dewar causing scattering and absorption effects on the steel walls. At the J-PARC, the extended beam transport before the beam-dump minimized the potential impact of this.

After subtraction ($n_{On} - n_{Off}$), the remaining signal was fitted to extract the fluorescence decay time-constant τ, with the results for individual acquisition sets at the KUR and J-PARC, shown in Figs. 12 and 13, respectively. Proper weighting of data points in the fit was difficult, as the experimental errors are an unknown combination of remaining electrical noise and shot-noise of the PMT, whose signal to noise ratio scales with the square-root of the number of photon events N. Considering this, a voltage error proportional to the square-root of the signal with a small added offset was assumed, with the offset accounting for electrical noise and to avoid negative weights. Nevertheless, the standard fit-error of τ was unreasonably small compared to the scatter of individual acquisitions. To get a more conservative and reliable error-estimate for τ, the fitting range
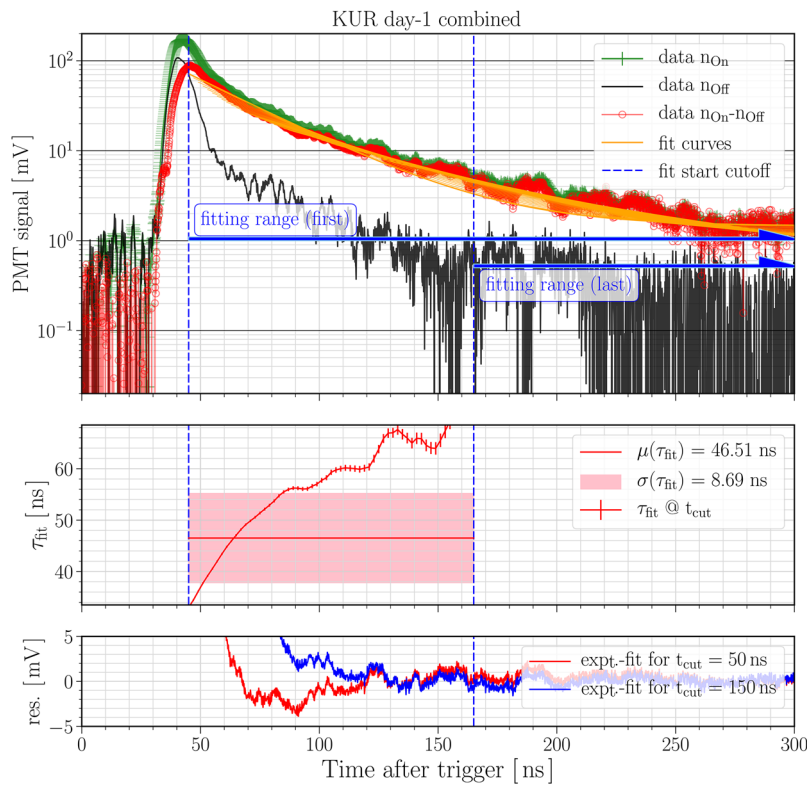
FIG. 10. Combined fluorescence signal of all acquisitions on the first day of the KUR experiment providing a comparison between neutron beam n_{On} and n_{Off} results. Fitting of the decay time-constant shows large variation depending on the included time range of data points, suggesting a multi-exponential decay. The n_{Off} result shows an unexplained slow decay with a similar time constant as the $^4He_2^*$ excimer.
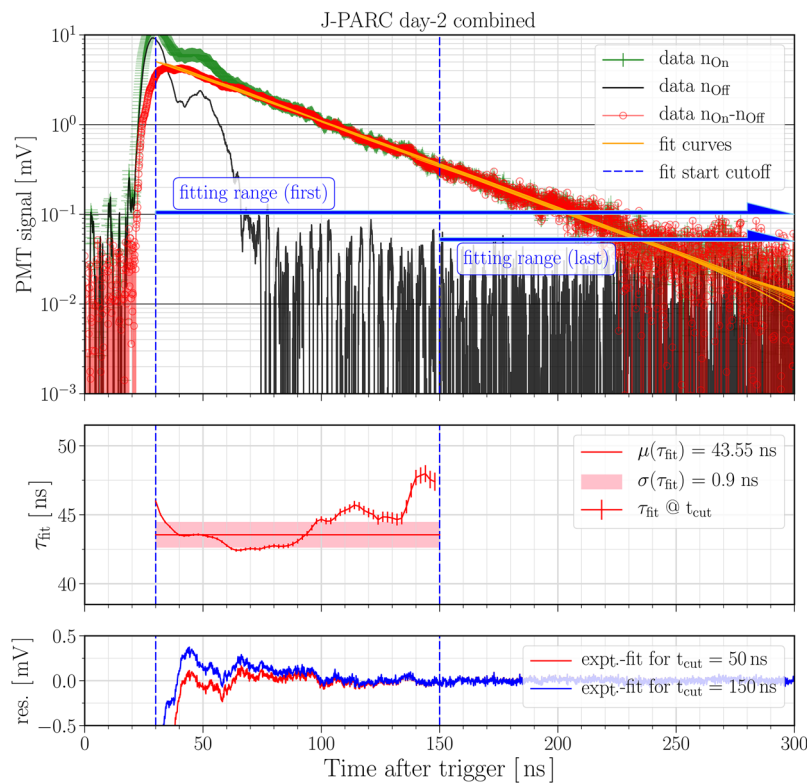

FIG. 11. Combined fluorescence signal of all acquisition on the second day of the J-PARC experiment. A smaller variation in the time-constant fitting results indicates a single-exponential decay. Furthermore, the "Off" result had only minimal contribution after the end of the laser pulse. A lower total signal strength compared to KUR results was mainly due to operation without preamplifier.
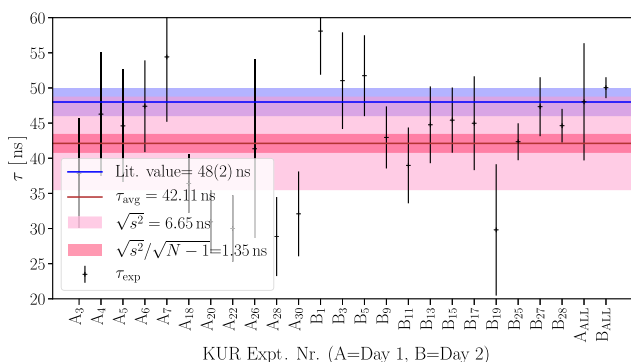
FIG. 12. Time constant results for KUR experiments and comparison with the literature value.[25]

was varied by selecting only the data points after an adjustable starting point indicated by the blue lines and arrows in these figures. The new fit-error was then calculated as the weighted standard-deviation from the ensemble of fit-values. This type of analysis was carried out both for daily integrated data (A_{ALL}, B_{ALL}) and for the individual acquisitions. In both cases, the average is slightly below the value from the literature.[25] For the KUR data, also a multi-exponential fit was attempted, but the signal quality was found to be insufficient to get a reliable convergence of the fit. Multi-exponential decays could occur if the laser excitation does not populate only a single excited state, but several different vibrational/rotational levels. These levels may decay each with their own lifetime to the upper level of the 640 nm fluorescence transition, causing a variation of the effective lifetime.

B. Laser energy and spot-size dependence

For imaging applications, saturation of the excitation transition is of high importance to maximize the fluorescence yield of each cluster of $^4He_2^*$ excimers. Only a few results with varying laser power and beam-diameter (spot-size) were taken due to the limited time and a lack of automated controls, which required entering
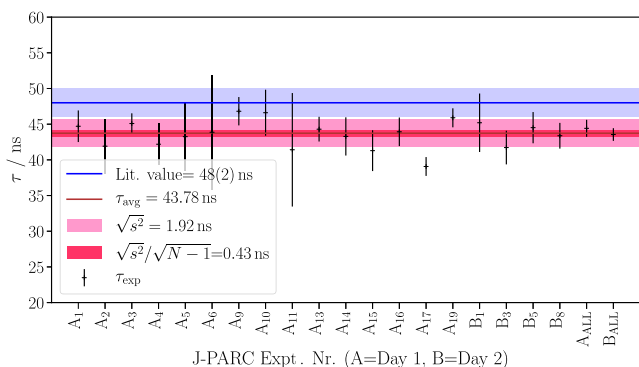

FIG. 13. Time constant results for J-PARC experiments. A lower range of fluctuations is seen here compared to the KUR.

the radiation area for adjustment. In addition, no suitable attenuator was prepared for the Ti:sa laser so that its output energy could only be varied by adjusting the pump intensity, which affected the output pulse duration as well. The intensity was estimated by dividing the pulse energy by the FWHM pulse duration and assuming an spot size of 2×4 mm^2 estimated with an IR viewer card. The PMT signal was integrated over the full time-span (0–500 ns) of each acquisition set, with the results shown in Fig. 14. Even though only three data points were available, a fit of the PMT signal P was attempted using a phenomenological model for two-photon absorption defined as $P(I) = \alpha \cdot I^2/(1 + I/I_{sat})^2$, i.e., the square of a simple two-level absorption model. Here, α is a proportionality constant, and $I_{sat} = 0.51(5)$ MW/cm^2 is the fitted saturation intensity. A more extensive dataset would be required to check the validity of the model.

The interaction volume was varied by adjusting the laser spot size with the telescope. As only a simple IR viewer card was used to judge the beam diameter and shape by eye a relatively large error has to be assumed. Results are shown in Fig. 15, indicating that while the $^4He_2^*$ fluorescence signal increases with beam diameter, the laser related background is actually reduced. The increase in $^4He_2^*$ signal is a further confirmation that the two-photon transition is saturated, as otherwise a flat or decreasing trend would be expected.

C. Repumping laser and wavelength dependence

The impact of the repumping lasers was evaluated, as shown in Fig. 16. Without repumping lasers (all off), the $^4He_2^*$ signal was a factor five lower than with repumping lasers. The 1064 nm laser had a slightly stronger effect than the 1085 nm laser and both repump lasers combined were again slightly better. Thus, for the low repetition rates used in this experiment (15 Hz), a single repump laser seems sufficient; however, at higher rates, this may change as there is less time available in between laser pulses for the repumping process to occur. It was also verified that the $^4He_2^*$ signal was influenced
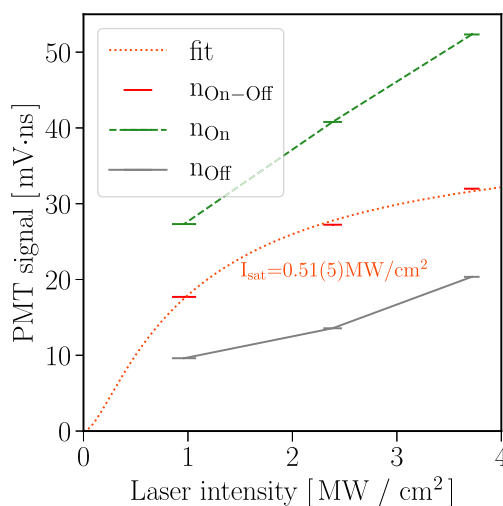

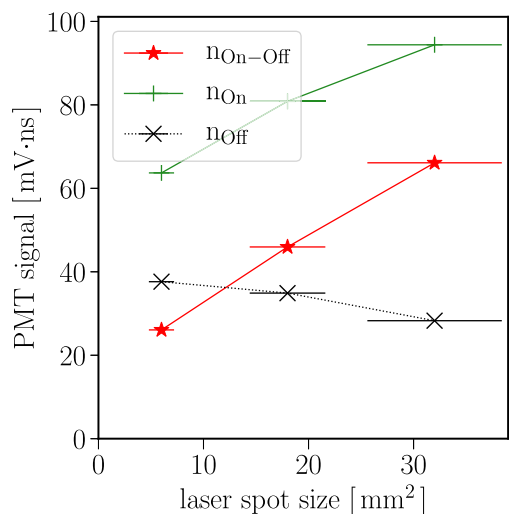**FIG. 14**. Dependence of the integrated PMT signal on laser intensity.

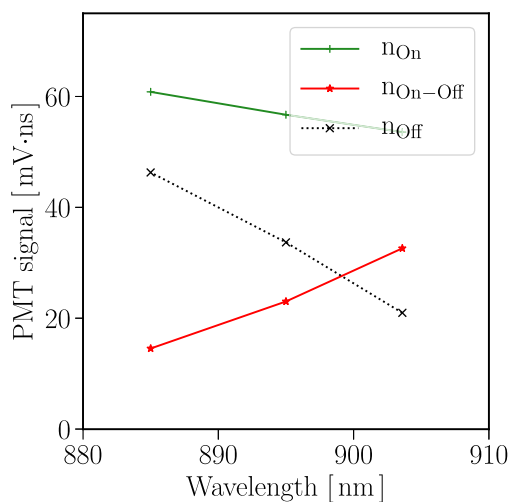**FIG. 15**. Dependence of fluorescence signal on laser spot size.

FIG. 17. Signal dependence on Ti:sapphire laser wavelength.

by the excitation laser's wavelength, with results given in Fig. 17. It was observed that the $^4He_2{}^*$ signal dropped when tuning away from the expected excitation wavelength of 905 nm. In contrast, the background signal (n_{Off}) was found to increase substantially, suggesting a different origin of this signal.

D. Effect of neutron beam

The general trend of excimer fluorescence signal intensity against the neutron beam flux was already discussed in our previous article[31] and is once again shown in Fig. 18. Here, the integrated PMT fluorescence signal against the relative neutron beam intensity is shown, adjusted via the collimators, as described in Table I.
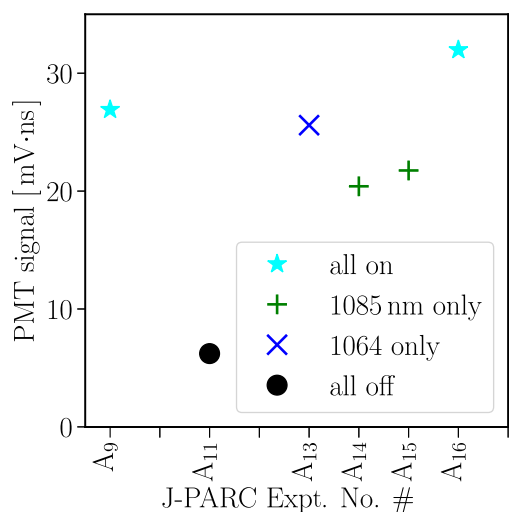
A proportional increase with neutron beam intensity is observed. To distinguish production of excimers via neutron absorption or γ-ray scattering (compton recoils), the same measurements were also performed, while the B_4C neutron blocker was introduced. With blocker inserted the signal drops to about 40% of the original level. This blocker was previously presumed to block only the neutron beam and be transparent for γ-rays.[31] However, after further consideration, it was concluded that it also attenuates the γ-ray intensity by a significant fraction.

Typically, γ-rays are emitted by structural components in the upstream beam-line so that their energies are expected to lie in the 1–10 MeV range. According to measurements using ^{137}Cs and ^{60}Co sources,[38] the absorption of 10 mm thickness B_4C is around 10% in this energy range. More importantly, the blocker had a 100 mm thickness high density polyethylene (HDPE, 0.95 g/cm^3) backing for neutron moderation, which has a similar attenuation coefficient,
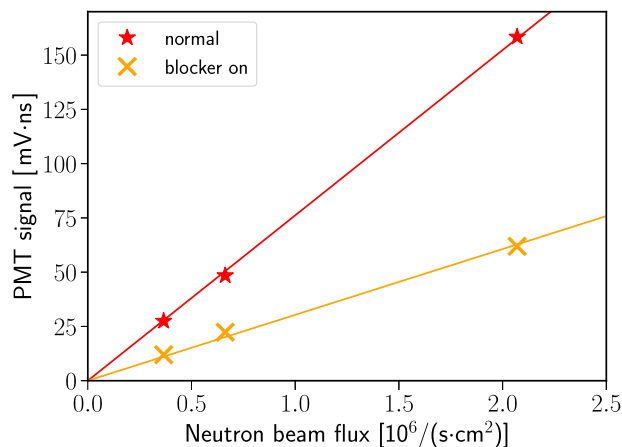

FIG. 16. Repump laser effect for both cw lasers.

FIG. 18. Fluorescence signal dependence on the neutron beam flux.

resulting in a combined (HDPE + B$_4$C) γ-transmission at 1 MeV of only 43%, based on calculations using cross sections from the XCOM database.[39] The attenuation of the neutron beam by the blocker may also reduce those γ-rays generated downstream by neutron induced reactions with material of the Dewar or surrounding materials. Another complication is the creation of prompt 0.48 MeV γ-rays by the neutron-capture reaction of Boron itself. A different blocker material such as lithium fluoride (LiF), which does not emit γ-rays, could be tried in a future experiment. Considering all of the above, the interpretation from our previous article,[31] that the main contribution to the generation of the excimers originates from the neutron capture reaction and not from γ-rays is not warranted anymore and additional investigations will be required to better control these factors.

There are a few possible explanations for a smaller than expected fraction of neutron-generated excimers. In dilute solutions of ^{3}He in superfluid ^{4}He, ^{3}He will follow mainly the normal fluid flow direction as well as diffusion and can lead to an ^{3}He concentration gradient along the flow direction. This effect is, for example, used in ^{4}He purifiers.[40] It has been observed as well using neutron tomography experiments[41] and could very likely affect our results, as the liquid helium was cooled using continuous pumping, resulting in a normal component flow toward the liquid helium surface, effectively flushing the ^{3}He out of the laser interaction region. This flush effect could, however, be partially counteracted by diffusive spread of the ^{3}He. Based on description of the diffusion of ^{3}He in liquid and superfluid helium in dilute conditions,[40,42,43] a few rough estimates can be made:

Assuming a liquid helium temperature of 1.8 K (lowest reached in the experiments) with a saturated vapor pressure of 1.64 kPa and a pumping speed of 600 l/min, the natural heat-load is calculated to be 610 mW. With a Dewar cross section of $\approx$200 cm^2 and under the assumption of homogeneous flow conditions, a normal fluid velocity of 0.2 mm/s was estimated. Inserting this result into Eq. (1) of the paper by Hendry,[40] along with the mass diffusion coefficient of $D \approx 10^{-4}$ cm^2/s,[44] the ^{3}He component will remain only in the top 1 mm layer of the liquid and thus overlap neither with the neutron beam nor the laser. As this flushing effect is only weakly depending on temperature, the only way to suppress this issue would be to reduce the heat load of the system by improving thermal insulation.

A second possibility is related to this normal flow as well as the size of the neutron beam and its pulsed emission in the J-PARC experiment. While the neutron-induced excimers are only produced in a 2 × 2 cm^2 area determined by the collimating slit before the Dewar, the γ-ray induced excimers may be produced in a much wider area. If there is a fast normal fluid component, the neutron-induced excimers may quickly escape from the laser-interaction region after a neutron pulse and would be lost for fluorescence emission, while the wider distributed γ-ray induced excimers would still cross the laser-interaction region during a longer time interval. This would essentially mean that the excimers would not accumulate in the interaction region over the 13 s lifetime of the excimer, and thus, the overall fluorescence signal would be reduced. Further possibilities include a lower than assumed original abundance ratio in the liquid helium, as well as preferred evaporation of ^{3}He during the cooling process due to its higher vapor pressure.

V. DISCUSSION AND OUTLOOK

A laser system has been developed for fluorescence measurements of ^{4}He$_2$* consisting of a short pulse Nd:YAG pumped Ti:sapphire laser and two cw repumping lasers. The system is sufficiently compact and stable for easy transportation to the neutron-beam facilities, allowing for a quick setup during the limited (1 day) preparation time before the start of the scheduled neutron beam-time. Datasets of two experimental runs at the J-PARC and KUR have been evaluated in detail. The excimer fluorescence lifetime was found to be slightly shorter than the literature value; however, as the discrepancy is small and both values have a similar error margin, it is difficult to judge which result is more accurate. Additional parameters, such as the wavelength, repumping, and intensity dependence, provide supplementary evidence that the main source of the fluorescence stems from the excimer, even though the results at the KUR indicate other possible sources of photons.

The presence of laser-related background signals is so far not fully explained but may originate from contamination on windows (which were not found to be completely clean). Furthermore, the direction of Fresnel reflections of the windows was observed using a visible laser source after the experiment concluded, showing relatively large reflection angles due to the imperfect alignment of the windows. This could result in partial beams of the laser hitting the internal Dewar walls, leading to the increased scatter. In future experiments, anti-reflection coatings and improved alignment will be considered. The inclusion of a second 640 nm bandpass-filter could be of advantage as well.

While there is some uncertainty as to whether the main reaction generating the excimer is neutron- or γ-induced, the total fluorescence signal could likely be drastically increased by enriching the helium with ^{3}He to increase the number of excimer clusters. However, to track individual clusters, a higher laser repetition rate to increase the fluorescence signal for visualization with a high sensitivity EMCCD or ICCD camera is needed. For this purpose, we are currently in the process of upgrading to a new higher rate pump laser. Individual telescopes for all three lasers will further improve the spatial overlap, and added automation controls will simplify future experiments. Installation of an optional cylindrical telescope to create a laser sheet for 2-D visualization is planned as well. However, based on the present results, the achieved pulse energy and duration are already sufficient, considering a possibly larger interaction volume for 3D flow tracking, and further increases in pulse energy will be investigated. If the sensitivity of excimer detection can be increased, this may advance the possibility of using liquid He as a directionally sensitive detector for light dark matter particles.[32]

To investigate whether there are flow dependent effects of the ^{3}He concentration or excimer laser interaction time, as proposed in Sec. IV D, we may attempt different pumping rates of the helium or the introduction of heater plates to modify the flow speed and direction of the normal component.

REFERENCES

[1] M. Nelkin, "What sense is turbulence an unsolved problem?," Science **255**(5044), 566–570 (1992).

[2] V. L'vov and I. Procaccia, "Turbulence: A universal problem," Phys. World **9**(8), 35 (1996).

[3] Y. Pomeau, "The long and winding road," Nat. Phys. **12**, 198–199 (2016).

[4] A. Tsinober, *An Informal Conceptual Introduction to Turbulence* (Springer, Dordrecht, 2009).

[5] C. F. Barenghi, L. Skrbek, and K. R. Sreenivasan, "Introduction to quantum turbulence," Proc. Natl. Acad. Sci. U. S. A. **111**(Supplement 1), 4647–4652 (2014).

[6] L. Skrbek, "Quantum turbulence," J. Phys.: Conf. Ser. **318**(1), 012004 (2011).

[7] L. Skrbek and K. R. Sreenivasan, "Developed quantum turbulence and its decay," Phys. Fluids **24**(1), 011301 (2012).

[8] M. S. Mongiovì, D. Jou, and M. Sciacca, "Non-equilibrium thermodynamics, heat transport and thermal waves in laminar and turbulent superfluid helium," Phys. Rep. **726**, 1–71 (2018), part of special issue: Non-equilibrium thermodynamics, heat transport and thermal waves in laminar and turbulent superfluid helium.

[9] A. J. Allen, N. G. Parker, N. P. Proukakis, and C. F. Barenghi, "Quantum turbulence in atomic Bose-Einstein condensates," J. Phys.: Conf. Ser. **544**(1), 012023 (2014).

[10] G. Baym, C. Pethick, and D. Pines, "Superfluidity in neutron stars," Nature **224**, 673 (1969).

[11] D. Page, M. Prakash, J. M. Lattimer, and A. W. Steiner, "Rapid cooling of the neutron star in cassiopeia a triggered by neutron superfluidity in dense matter," Phys. Rev. Lett. **106**, 081101 (2011).

[12] STAR Collaboration, "Global Λ hyperon polarization in nuclear collisions," Nature **548**(7665), 62–65 (2017), Letter.

[13] P. Sikivie and Q. Yang, "Bose-Einstein condensation of dark matter axions," Phys. Rev. Lett. **103**, 111301 (2009).

[14] L. Tisza, "Transport phenomena in helium II," Nature **141**, 913 (1938).

[15] L. Landau, "Theory of the superfluidity of helium II," Phys. Rev. **60**, 356–358 (1941).

[16] G. P. Bewley, D. P. Lathrop, and K. R. Sreenivasan, "Visualization of quantized vortices," Nature **441**, 588 (2006).

[17] T. Zhang and S. W. Van Sciver, "Large-scale turbulent flow around a cylinder in counterflow superfluid ^{4}He (He (II))," Nat. Phys. **1**, 36 (2005).

[18] R. J. Adrian, "Twenty years of particle image velocimetry," Exp. Fluids **39**(2), 159–169 (2005).

[19] M. Virant and T. Dracos, "3D PTV and its application on Lagrangian motion," Meas. Sci. Technol. **8**(12), 1539–1552 (1997).

[20] D. N. McKinsey, W. H. Lippincott, J. A. Nikkel, and W. G. Rellergert, "Trace detection of metastable helium molecules in superfluid helium by laser-induced fluorescence," Phys. Rev. Lett. **95**, 111101 (2005).

[21] J. Gao, A. Marakov, W. Guo, B. T. Pawlowski, S. W. Van Sciver, G. G. Ihas, D. N. McKinsey, and W. F. Vinen, "Producing and imaging a thin line of He_2^* molecular tracers in helium-4," Rev. Sci. Instrum. **86**(9), 093904 (2015).

[22] W. Kubo and Y. Tsuji, "Lagrangian trajectory of small particles in superfluid He II," J. Low Temp. Phys. **187**(5), 611–617 (2017).

[23] A. Marakov, J. Gao, W. Guo, S. W. Van Sciver, G. G. Ihas, D. N. McKinsey, and W. F. Vinen, "Visualization of the normal-fluid turbulence in counterflowing superfluid ^{4}He," Phys. Rev. B **91**, 094503 (2015).

[24] D. E. Zmeev, F. Pakpour, P. M. Walmsley, A. I. Golov, W. Guo, D. N. McKinsey, G. G. Ihas, P. V. E. McClintock, S. N. Fisher, and W. F. Vinen, "Excimers He_2^* as

[25] tracers of quantum turbulence in ^{4}He in the $T = 0$ limit," Phys. Rev. Lett. **110**, 175303 (2013).

[25] W. G. Rellergert, S. B. Cahn, A. Garvan, J. C. Hanson, W. H. Lippincott, J. A. Nikkel, and D. N. McKinsey, "Detection and imaging of He_2 molecules in superfluid helium," Phys. Rev. Lett. **100**, 025301 (2008).

[26] W. Guo, J. D. Wright, S. B. Cahn, J. A. Nikkel, and D. N. McKinsey, "Metastable helium molecules as tracers in superfluid ^{4}He," Phys. Rev. Lett. **102**, 235301 (2009).

[27] J. W. Keto, F. J. Soley, M. Stockton, and W. A. Fitzsimmons, "Dynamic properties of neutral excitations produced in electron-bombarded superfluid helium II. Afterglow fluorescence of excited helium molecules," Phys. Rev. A **10**, 887–896 (1974).

[28] G. Tastevin, B. Glowacz, and P.-J. Nacher, "Using a cw 465 nm laser to probe metastable He_2 Molecules," J. Low Temp. Phys. **158**(1), 339 (2009).

[29] B. Glowacz, "Detection of metastable He$_2$∗ molecules in helium plasma," Ph.D. thesis, Université Paris 6 Pierre et Marie Curie; Jagiellonian University, 2011, URL: https://tel.archives-ouvertes.fr/tel-01360241/document.

[30] M. La Mantia, P. Švančara, D. Duda, and L. Skrbek, "Small-scale universality of particle dynamics in quantum turbulence," Phys. Rev. B **94**, 184512 (2016).

[31] T. Matsushita, V. Sonnenschein, W. Guo, H. Hayashida, K. Hiroi, K. Hirota, T. Iguchi, D. Ito, M. Kitaguchi, Y. Kiyanagi, S. Kokuryu, W. Kubo, Y. Saito, H. M. Shimizu, T. Shinohara, S. Suzuki, H. Tomita, Y. Tsuji, and N. Wada, "Generation of $^4He_2^*$ clusters via neutron-^{3}He absorption reaction toward visualization of full velocity field in quantum turbulence," J. Low Temp. Phys. **196**, 275 (2018).

[32] W. Guo and D. N. McKinsey, "Concept for a dark matter detector using liquid helium-4," Phys. Rev. D **87**, 115001 (2013).

[33] A. Tarasov and H. Chu, "Generation of pulses with sub-nanosecond duration and sub-joule energy in gain-switched Ti:Sapphire lasers," Opt. Express **27**(3), 3574–3582 (2019).

[34] E. Räikkönen, M. Kaivola, and S. Buchter, "Compact supercontinuum source for the visible using gain-switched Ti:Sapphire laser as pump," J. Eur. Opt. Soc. - Rapid Publ. **1**, 06012 (2006).

[35] J. J. Zayhowski and A. L. Wilson, "Miniature pulsed Ti:sapphire laser system," in *Summaries of Papers Presented at the Lasers and Electro-Optics, CLEO '02, Technical Digest* (Optical Society of America, 2002), Vol. 1, p. 428, available at https://www.osapublishing.org/abstract.cfm?uri=CLEO-2002-CWN5.

[36] F. Salin and J. Squier, "Gain guiding in solid-state lasers," Opt. Lett. **17**(19), 1352–1354 (1992).

[37] Y. Saito, S. Sekimoto, M. Hino, and Y. Kawabata, "Development of neutron radiography facility for boiling two-phase flow experiment in Kyoto university research reactor," Nucl. Instrum. Methods Phys. Res., Sect. A **651**(1), 36–41 (2011), part of special issue: Proceeding of the Ninth World Conference on Neutron radiography ("The Big-5 on Neutron Radiography").

[38] B. Buyuk and A. Beril Tugrul, "Gamma and neutron attenuation behaviours of boron carbide–silicon carbide composites," Ann. Nucl. Energy **71**, 46–51 (2014).

[39] M. J. Berger, J. H. Hubbell, S. M. Seltzer, J. S. Coursey, J. Chang, R. Sukumar, D. S. Zucker, and K. Olsen, online https://doi.org/10.18434/T48G6X, 2010 (last accessed September 11, 2019).

[40] P. C. Hendry and P. V. E. McClintock, "Continuous flow apparatus for preparing isotopically pure ^{4}He," Cryogenics **27**(3), 131–138 (1987).

[41] M. E. Hayden, G. Archibald, P. D. Barnes, W. T. Buttler, D. J. Clark, M. D. Cooper, M. Espy, R. Golub, G. L. Greene, S. K. Lamoreaux, C. Lei, L. J. Marek, J.-C. Peng, and S. I. Penttila, "Neutron-detected tomography of impurity-seeded superfluid helium," Phys. Rev. Lett. **93**, 105302 (2004).

[42] R. P. Behringer and H. Meyer, "Diffusive relaxation processes in liquid ^{3}He-^{4}He mixtures. II. Superfluid phase," J. Low Temp. Phys. **46**(5), 435–450 (1982).

[43] D. Murphy and H. Meyer, "Heat transport in dilute mixtures of ^{3}He in superfluid ^{4}He," J. Low Temp. Phys. **107**(1), 175–196 (1997).

[44] S. K. Lamoreaux, G. Archibald, P. D. Barnes, W. T. Buttler, D. J. Clark, M. D. Cooper, M. Espy, G. L. Greene, R. Golub, M. E. Hayden, C. Lei, L. J. Marek, J.-C. Peng, and S. Penttila, "Measurement of the ^{3}He mass diffusion coefficient in superfluid ^{4}He over the 0.45–0.95 K temperature range," Europhys. Lett. (EPL) **58**(5), 718–724 (2002).